Accepted Manuscript
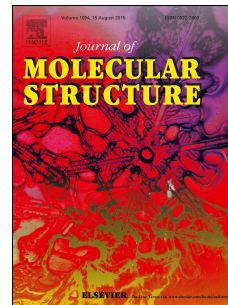
Charge-transfer complexes of hypoglycemic sulfonamide with π-acceptors: Experimental and DFT-TDDFT studies

Sara Soltani, Pierre Magri, Marek Rogalski, Mekki Kadri

Please cite this article as: S. Soltani, P. Magri, M. Rogalski, M. Kadri, Charge-transfer complexes of hypoglycemic sulfonamide with π-acceptors: Experimental and DFT-TDDFT studies, *Journal of Molecular Structure* (2018), doi: 10.1016/j.molstruc.2018.07.074.

Graphical abstract

Gliclazide (GLC)

CHCl₃

DDQ

π→π*

[(GLC)(DDQ)]

CHCl₃

TCNE

[(GLCTCNE)]

Charge-transfer complexes of hypoglycemic sulfonamide with π-acceptors: Experimental and DFT-TDDFT studies

Sara Soltani[1], Pierre Magri[2], Marek Rogalski[2], and Mekki Kadri[1*]

[1]Laboratoire de Chimie Physique, Université 08 Mai 45, BP401, Guelma 24000, Algeria.

[2]Laboratoire de Chimie et de Physique Approches Multi-échelles des Milieux Complexes, Université de Lorraine, 1 Boulevard Arago, Technopole, 57070 Metz, France.

[*] Corresponding author Tel +213772749499; E-mail address: mekkadri@gmail.com (M.kadri)

Abstract

Charge-transfer interactions (CT) between the electron donor gliclazide (GLC) and the π-acceptors 2,3-dichloro-5,6-dicyano-1,4-benzoquinone (DDQ) and tetracyanoethylene (TCNE) were studied in a chloroform solution and in the solid state. The CT complexes were discussed in terms of formation constants (K_{CT}), molar extinction coefficients (ε_{CT}), standard reaction quantities ($\Delta G°$, $\Delta H°$, and $\Delta S°$), oscillator strength (f), transition dipole moment (μ_{EN}), and ionization potential (I_p). The limits of detection (LOD) and limits of quantification (LOQ) have also been reported. The stoichiometry of these complexes was found to be in a 1:1 molar ratio. The formed solid CT complexes were also synthesized and characterized using electronic methods, FT-IR, ^{1}H and ^{13}C NMR spectroscopy. Thermogravimetric analysis techniques (TGA/DTA) and differential scanning calorimetry (DSC) were used to determine the thermal stability of the synthesized CT complex. The kinetic parameters (ΔG^*, ΔH^*, and ΔS^*) were calculated from thermal decomposition data using the Coats-Redfern method. Moreover, density functional theory (DFT) studies are discussed for the charge transfer complex GLC-TCNE, using the B3LYP with 6-311++G (d, p) basis set. The harmonic vibrational frequencies were calculated, and the scaled values have been compared with experimental FT-IR spectra. The calculated ^{1}H and ^{13}C NMR chemical shifts using the GIAO method showed good correlations with the experimental data. The theoretical UV-visible spectrum of the compound and the electronic properties, such as HOMO and LUMO energies, were performed using the time-dependent (TD-DFT) approach with CAM-B3LYP, employing the 6-311++G (d, p) basis set, and good agreement with the theoretical and experimental UV-visible data was found.

Key words: Complex, Charge transfer, Gliclazide, DDQ, TCNE, π-acceptors, DFT, TDDFT.

1. Introduction

The study of the charge-transfer (CT) or proton-transfer complexation of drugs with small molecule acceptors is currently of considerable importance and have become a popular area of research because of their individual physical and chemical properties and varied range of applications [1]. The chemistry of these interactions has received great attention in pharmacology, life sciences, medicine, and chemistry, and certain π-acceptors have successfully been utilized in pharmaceutical analysis of drugs in pure form or in pharmaceutical preparations. During the last decade, many studies were focused on drug-acceptor interactions in solution and in solid-state. The drug-acceptor complexation is an important technique that is simpler, cheaper, and more efficient than the methods of drug determination described in the literature. Also, the study of this complexation process play extremely important roles in many processes; therefore, understanding these interactions is significant for the recognition of drug-receptor binding and the drug's mechanism of action as well as for obtaining quantitative estimates of drugs [2-13].

Gliclazide, (1-(Hexahydrocyclopenta[c]pyrrol-2(1H)-yl)-3-[(4-methylphenyl)sulfonyl]urea) (GLC) [14] (Figure 1 in the electronic supplementary materials), is a second-generation sulfonylurea derivative widely used to treat non-insulin-dependent diabetes mellitus (NIDDM). The drugs in this class act by stimulating the secretion of insulin from pancreatic β cells [15]. They differ in dose, rate of absorption, duration of action, route of elimination, and binding site on the target receptor for pancreatic β cells [16]. GLC has antioxidant properties, and may reduce the harmful consequences of oxidative stress in diabetic patients [17]. It also has a low incidence of severe hypoglycemia and other hemobiological effects [18]. It is administered orally and has a duration of action from 12 to 24 h. Due to its shorter duration of action compared with chlorpropamide or glibenclamide, it may be more appropriate for elderly patients who are prone to hypoglycemia with longer-acting sulfonylureas [19].

GLC has been the subject of important research due to its reactivity, for example, its interactions with macromolecules (CDs and polymers) [20-25], proteins and enzymes [26-30], other drugs leading to drug-drug interactions [31, 32], and metal ions [33-35] have been studied. However, to our knowledge, there has been no study on the ability of GLC to form charge transfer (CT) complexes reported in the literature. In addition, the properties of CT complexes formed with donors containing nitrogen, sulfur, and oxygen atoms have become increasingly important in recent years [36-48].

The objective of the first aspect of this study was to investigate the interactions between a GLC donor with 2,3-dichloro-5,6-dicyano-1,4-benzoquinone (DDQ) and tetracyanoethylene

(TCNE) as π-acceptors (Figure 1 in the electronic supplementary materials). Analyzing the complexes in a chloroform solution by spectrophotometry allowed for the determination of the stoichiometry, stability constants, molar extinction coefficients, thermodynamic quantities ($\Delta G°$, $\Delta H°$, and $\Delta S°$), and spectroscopic properties, such oscillator force (*f*), transition dipole moment (μ_{EN}), and ionization potential (I_p). The limit of detection (LOD) and limit of quantification (LOQ) have been reported and were in accordance with the guidelines of the International Conference on Harmonization (ICH) [49]. The solid-state complexes were synthesized and characterized by FT-IR, ^{1}H NMR, and ^{13}C NMR spectroscopy, and by TGA/DTA and DSC thermal analyses.

In the second part of this work, we report the results from DFT and TD-DFT calculations on the GLC-TCNE complex. The electronic properties and HOMO and LUMO energies were determined for the optimized charge-transfer complex. The theoretical UV visible, FT-IR, and ^{1}H and ^{13}C NMR spectra were compared with those obtained experimentally.

2. Experimental

2.1. Materials and instrumentation

GLC (1-(Hexahydrocyclopenta[c]pyrrol-2(1H)-yl)-3-[(4-methylphenyl)sulfonyl]urea), DDQ, and TCNE were obtained from Aldrich Chemical Co. and were used without modification. Spectroscopic-grade solvents (methanol and chloroform) were purchased from Fluka or Prolabo.

The electronic absorption spectra were recorded between 600 and 200 nm using a Jasco UV-530 spectrophotometer equipped with a Jasco EHC-477S thermostat ($\pm0.1°C$) with 1 cm quartz cells.

The FT-IR spectra of the reactants and the formed complexes were recorded using a spectrophotometer (Spectrum One FT-IR spectrometer of Perkin Elmer).

The ^{1}H and ^{13}C NMR spectra were collected on a Bruker Advance spectrometer operating at 400 MHz. The measurements were performed at room temperature using DMSO-d_6 (dimethylsulfoxide, d_6) as solvent and TMS (tetramethylsilane) as an internal reference.

Differential scanning calorimetry (DSC) was performed using a DSC Q2000 V24.10 Build 122 instrument, between 25 and 275 °C with a heating rate of 10°C min^{-1}.

The TGA/DTA thermograms were detected using a TGA Q500 V20.13 Build 39 instrument, from 0 to 600 °C with a heating rate of 10°C min^{-1}.

2.2. General analytical procedures

2.2.1. Photometric titration

In order to determine the stoichiometry of the complexes, photometric titration measurements were taken for the reactions between the GLC donor and each of the acceptors, DDQ and TCNE, at 25°C according to the method described in the literature [50, 51]. The measurements were obtained by keeping the concentration of the GLC donor constant and modifying that of the acceptors over a wide range, where the molar ratio of donor:acceptor varied from 1: 0.25 to 1: 4. The absorbances of the CT complexes were measured at 266 nm and 259 nm for GLC-DDQ and GLC-TCNE, respectively. Stoichiometry was determined by plotting absorbance as a function of molar ratio.

2.2.2. Construction of calibration curves

Equivalent aliquots of standard GLC (4–48 µg mL^{-1} for GLC-DDQ (method A) and 2–36 µg mL^{-1} for GLC-TCNE (method B)) were transferred into two separate series of calibrated 3 mL vials. For each series, 1 mL of 0.1% DDQ or TCNE was added to each vial. The test vials were swirled for 5 min and the solutions were filled to the mark with chloroform. The absorbances were measured at 266 nm and 259 nm for GLC-DDQ and GLC-TCNE, respectively.

2.3. Preparation of solid complexes

Equimolar amounts of the donor and acceptor were separately dissolved in the minimum volume of a mixed methanol/chloroform mixture (1:9, v/v). The mixture was stirred continuously for 24 h at room temperature. After a slow evaporation, the colored solid complexes were washed with a small amount of solvent, dried under vacuum, and stored on anhydrous calcium chloride.

2.4. Computational details

All the computations were performed using the Gaussian09 program package [52], and GaussView [53] was used for visualization of the structures and simulation of the vibrational, UV-vis, and ^{1}H and ^{13}C NMR spectra. Two possible structures, S1 and S2, could be proposed for the complex of GLC with TCNE. However, the discussions will only be of the most stable structure.

The geometrical structures of GLC, TCNE, S1, and S2 were optimized at the DFT/B3LYP level of theory, employing the 6-311++G (d, p) basis set in vacuum for GLC and TCNE, and

in chloroform as a solvent for the two proposed structures, S1 and S2. The nature of the excitations in the observed UV-Visible spectrum of the most stable structure has been studied using time-dependent density functional theory (TD-DFT) in chloroform solvent using CAM-B3LYP/6-311++G (d, p). In addition, the electronic properties, such as HOMO and LUMO energies, were determined. A simulated FT-IR spectrum was studied by applying the B3LYP/6-311++G (d, p) method. The ^{1}H and ^{13}C NMR chemical shifts were calculated with the B3LYP/6-311++G (d, p) level by using the gauge invariant atomic orbital (GIAO) [54] approach in DMSO. Default convergence criteria have been applied. The solvent effect for all calculations in chloroform or DMSO was considered by using the integral equation formalism polarizable continuum model (IEFPCM).

3. Results and discussion

3.1. Liquid state analyses

3.1.1. Electronic spectra

The spectrophotometric visualization of the interaction of GLC with each acceptor was studied in chloroform solution at 25°C in the range 220–400 nm. The progressive addition of the acceptor to the donor solution caused changes in the spectra and batho- or hypsochromic displacements (increases in the intensity of the absorption band or appearance of a new band in the region where neither the acceptor nor the donor absorbs) that are characteristic of the formation of CT complexes were observed [55].

Figure 1A shows the electronic absorption spectra of GLC in chloroform with various concentrations of DDQ. With the addition of DDQ, we observed the appearance of a new band at 266 nm with an increase in the absorbance at 350 nm.

Similarly, Figure 1B shows the changes to the donor spectra in chloroform solution as a function of the gradual addition of TCNE solution. We observed the appearance of a new absorption band at 259 nm, and an isopiestic point at 311 nm.
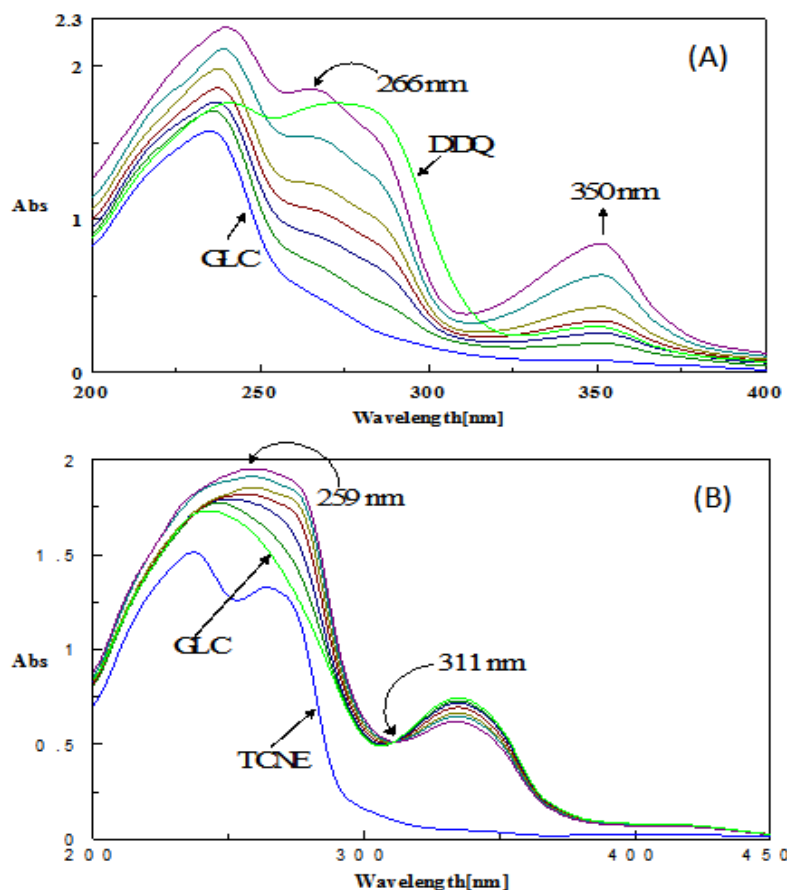
Fig. 1.

These results indicate the formation of CT complexes between the GLC molecule and each of the acceptors (DDQ and TCNE). The stoichiometry determined by photometric titration at 266 nm for GLC-DDQ and 259 nm for GLC-TCNE, showed that the donor:acceptor molar ratio was 1:1 (Figure 2 in the electronic supplementary materials).These results were also supported by the FTIR, ^{1}H NMR, ^{13}C NMR, and thermal analysis results to confirm the formation of [(GLC)(DDQ)] and [(GLCTCNE)] complexes.

3.1.2. Determination of complex stability constants

The Benesi-Hildebrand equation (Eq (1)) [56] was used to calculate the stability constants (K) and molar extinction coefficients (ε_{CT}) for the two complexes in chloroform at 25 °C:

$$\frac{C_a^0 C_d^0}{Abs} = \frac{1}{K\varepsilon_{CT}} + \frac{C_d^0}{\varepsilon_{CT}} \tag{1}$$

where C_a and C_d are the initial concentrations of the acceptors (DDQ and TCNE) and the donor (GLC), respectively. Abs is the absorbance of the donor-acceptor mixture at the wavelength λ_{CT} (266 nm for GLC-DDQ and 259 nm for GLC-TCNE).

Eq (1) is valid under the condition $C_d \gg C_a$, where $C_a C_d$ /Abs values for the 1:1 CT complex were plotted against the corresponding C_d values. Straight lines were obtained with a slope of $1/\varepsilon_{CT}$ and an intercept of $1/K\varepsilon_{CT}$, as shown in (Figure 3 in the electronic supplementary materials). The values of K_{CT} and ε_{CT} associated with the CT complexes are given in (Table 1 in the electronic supplementary materials).

3.1.3. Determination of the thermodynamic parameters of the CT complexes

Evaluation of the stability constants K of the complexes at four different temperatures (288, 293, 298, and 303 K) allowed determination of the thermodynamic parameters ($\Delta H°$, $\Delta S°$) using thevan't Hoff equation [57, 58] in terms of lnK as a function of 1/T (Eq(2)).

$$\ln K = -\frac{\Delta H^0}{RT} + \frac{\Delta S^0}{R} \tag{2}$$

The plot of lnK versus 1/ T for the two CT complexes of GLC with DDQ or TCNE is shown in (Figure 4 in the electronic supplementary materials). The linear plots had correlation coefficients exceeding 0.97. The enthalpies and entropies of the complexes were determined from the slopes and intercepts, respectively.

The free energy changes ($\Delta G°$) were calculated according to the equation:

$$\Delta G° = \Delta H° - T\Delta S° = -RT \ln K \tag{3}$$

where $\Delta G°$ is the free energy change of the CT complexes, R is the gas constant (8.314 Jmol^{-1}K^{-1}), and T is the ambient temperature in Kelvin. The obtained results are listed in Table 1.

Table 1.

	[(GLC)(DDQ)]	[(GLCTCNE)]
$\Delta H°$ (kj mol^{-1})	-32.18	-37.76
$\Delta S°$ (j mol^{-1} K^{-1})	-37.12	-24.01
$\Delta G°$ (kj mol^{-1})	-21.12	-30.61

The values of the thermodynamic parameters listed in Table 1 show that the CT reactions were exothermic and all thermodynamically favorable (spontaneous $\Delta G° < 0$).

The high values of free enthalpies, and therefore stability constants, indicate that the interactions between the GLC donor and the acceptors (DDQ, TCNE) are strong.

3.1.4. Determination of spectroscopic and physical data

Analysis of spectrophotometric spectra allows the determination of some spectroscopic and physical parameters that characterize the CT phenomena such as the oscillator strength (*f*), transition dipole moment (μ_{EN}), and ionization potential (I_P).

Determination of oscillator strength (f)

The oscillator*strength (f)* is estimated from the basic formula [59] :

$$f = 4.32 \times 10^{-9} \int \varepsilon dv \tag{4}$$

where $\int \varepsilon dv$ is the area under the curve of the molar extinction coefficient of the absorption band in question versus frequency. As a first approximation:

$$f = 4.32 \times 10^{-9} \varepsilon_{CT} \Delta v_{1/2} \tag{5}$$

where ε_{CT} is the maximum molar extinction coefficient of the band, and $\Delta v_{1/2}$ is the half-bandwidth in cm^{-1} (i.e., the bandwidth at half of the maximum extinction coefficient).

The calculated oscillator strength values (Table 2) indicate a strong interaction between the GLC donor and acceptors (DDQ or TCNE) with relatively high probabilities of CT transitions. This is also supported by the relatively large amount of heat formation.

Determination of transition dipole moment (μ_{EN})

The transition dipole moment (μ_{EN}) of each complex was calculated from Eq (6) [60]:

$$\mu_{EN} = 0.0952 [\varepsilon_{CT} \Delta v_{1/2} / \Delta v]^{1/2} \tag{6}$$

where $\Delta v \approx v_{CT}$ at ε_{CT} and μ_{EN} is defined as $-e \int \Psi_{ex} \sum_i r_i \Psi_g d\tau$.

Determination of the ionization potential (I_P) of the donor

The ionization potential (I_P) of the GLC donor in each complex was calculated using the empirical equation derived by Aloisi and Pignataro, and shown in Eqs (7) and (8) [61]:

$$I_P (eV) = 5.76 + 1.53 \times 10^{-4} v_{CT} \text{ for DDQ} \tag{7}$$

$$I_P (eV) = 5.21 + 1.65 \times 10^{-4} v_{CT} \text{ for TCNE} \tag{8}$$

where v_{CT} is the wavenumberin cm^{-1} that corresponds to the CT band formed from the donor-acceptor interaction. The electron-donating power of a donor molecule is measured by its

ionization potential, which is the energy required to remove an electron from the highest occupied molecular orbital.

The calculated oscillator strengths, transition dipole moments, and ionization potentials for both complexes are summarized in (Table 2).

Table 2.

Complex	λ_{CT} (nm)	ε_{CT}	f	μ_{EN}	I_P
[(GLC)(DDQ)]	266	4.79×10^4	230.02	29,46	11.5
[(GLCTCNE)]	259	2.03×10^4	87.7	19.18	11.6

3.1.5. Linearity

By using the above procedure, linear regression equations were obtained. The regression plots showed that the analytical response of the two methods was linearly dependent on the concentration of GLC over the ranges cited in (Table 2 in the electronic supplementary materials). Linear regression analysis of the data gave the following equations. For method A, Y=0.00132X–0.000109, R=0.99, and for method B, Y=0.00135X–0.0016, R=0.99 (where Y is the absorbance, X is the concentration of the drug ($\mu g\ mL^{-1}$), and R is the correlation coefficient).

3.1.6. Limits of detection and quantification

The limits of detection (LOD) and limits of quantification (LOQ) were according to the guidelines of the International Conference on Harmonization (ICH) [49].LOD and LOQ were calculated using the following equations [62]:

$$LOD = 3.3 \times S/b \tag{9}$$

$$LOQ = 10 \times S/b \tag{10}$$

where S is the standard deviation of the intercept of the regression line and b is the slope of the calibration curve [62].

The LOD and LOQ values obtained and shown in (Table 2 in the electronic supplementary materials) are relatively low, indicating a high measurement sensitivity of GLC using the proposed methods.

9

3.2.Solid state analyses

3.2.1. IR spectra

The experimental infrared spectra of GLC and its corresponding complexes, [(GLC)(DDQ)] and [(GLCTCNE)], are shown in (Figure 5 in the electronic supplementary materials). The principal absorption band assignments in the infrared spectra are reported in (Table 3 in the electronic supplementary materials). Donor interaction with each of the acceptors is evidenced by the presence of their main infrared bands in the spectra of the resulting complexes. Comparing the spectra of the free reactants, the GLC donor, DDQ, and TCNE acceptors with the spectra of their corresponding complexes (Figure 5 in the electronic supplementary materials) enabled the detection of changes in the frequency and/or intensity of the bands following formation of the complexes.

The FT-IR spectrum of the [(GLC)(DDQ)] (Figure 5D in the electronic supplementary materials) complex indicated that the band resulting in ν (C≡N) vibration of the free acceptor DDQ changed in frequency and decreased in intensity in the complexes upon CT complexation. Free DDQ shows two vibrations (ν)(C≡N) at 2299.76 and 2232.43 cm^{-1}, while in its complex, ν (C≡N) appears at the lower wavenumber value (2254.84 cm^{-1}). It is clear that ν (C≡N) of DDQ is decreasing during complexation. The characteristic band of the ν (NH) group observed at 3267.96 cm^{-1} in the free donor (GLC) is shifted to 3191.60 cm^{-1} in the complex, and its intensity as decreased. These observations clearly confirm that the NH group in the GLC donor and the C≡N group in the DDQ acceptor participated in the complexation process. The groups of bands assigned to the vibrations ν (C=O) and ν(C=C) appear at 1699.17 cm^{-1} and 1551.80 cm^{-1}, respectively, in the free DDQ, with a shift towards the higher wavenumbers at 1747.67 cm^{-1} and 1574.94 cm^{-1}, respectively.

Because the acceptor does not contain acidic centers and the complex spectrum shows that the characteristic C= C band is affected, it can be concluded that the molecular complex is formed by $\pi \rightarrow \pi^*$ and/or n$\rightarrow \pi$ * charge migrations from the donor HOMO to the LUMO of the acceptor. The $\pi \rightarrow \pi^*$ CT complex is formed via the benzene rings (electron-rich group) of the GLC and DDQ reagents [63]. The cyano group (C≡N) is an electron-withdrawing group that exists in the DDQ in a conjugated binding system. The two CN groups in the acceptor withdraw the electrons from the aromatic ring, and such a process will make the aromatic ring an electron-accepting region. The π^*–CN electron density appears to increase and more readily accept a proton from the donor due to the electron-withdrawing process and the conjugated electron system. Thus, the mode of interaction between GLC and the acceptor DDQ also occurs by the migration of a H$^+$ ion to one of the cyano groups in the DDQ

10

acceptor to form a positive ion (–C≡N$^+$H), which associates with the (–N$^-$) anion to form ion pairs [64, 65].

The FT-IR spectrum of the GLC complex with the TCNE (Figure 5E in the electronic supplementary materials) shows that the ν (N–H) vibration of the GLC does not undergo any significant change following the donor-acceptor interaction, while the vibrations ν (C≡N) observed at 2277.51 and 2243.81 cm^{-1} in the free TCNE are affected in intensity, shifted, and observed as a triplet at 2300.87, 2201.50, and 2170.78 cm^{-1} in the complex spectrum. The characteristic bands of C=C and C–C observed at 1685.21 and 1195.05 cm^{-1} of free TCNE, respectively, are shifted to 1634.79 and 1229.79 cm^{-1}. These findings suggest the possibility of involving a covalent bond between GLC and TCNE missing one of its cyano (C≡N) groups.

3.2.2. ^{1}H and ^{13}C NMR

The GLC molecule possesses two NH groups that may be involved in donor-acceptor interactions. As GLC is asymmetric, it is useful to determine which of the two is more favorable in a 1:1 stoichiometric reaction. Electronic and steric factors will affect which group is more favorable, and this was determined by ^{1}H and ^{13}C NMR. To investigate the changes occurring during the complexation reactions, the ^{1}H and ^{13}C NMR chemical shifts (δ ppm) of the free GLC donor [14] and the ^{13}C NMR chemical shifts (δ ppm) of free DDQ and TCNE acceptors [66, 67] are presented in (Figures 6 and 7 respectively in the electronic supplementary materials).

The chemical shifts of the SO$_2$–NH–CO and CO–NH–N protons in GLC were at 6.4 and 8.8 ppm, respectively.

The spectrum and the ^{1}H NMR chemical shifts for the charge-transfer complex formed between GLC and DDQ are shown in (Figure 8A in the electronic supplementary materials). The spectrum indicates the disappearance of the SO$_2$-NH-CO proton signal of the free donor (GLC). Instead, a new peak is observed at 4.01 ppm in the complex spectrum that is attributed to the ($^+$NH) proton. This new signal was not observed in the free GLC spectrum, indicating the proton migration of SO$_2$–NH–CO to one of the two cyano groups of the DDQ acceptor. This migration resulted in the formation of a positive ion (–C≡N$^+$ H) (Formula 1, Figure 2A). These findings confirm that the NH of GLC and CN of DDQ are primarily involved in the formation of the CT complex between GLC and DDQ, as shown in Figure 2A.

Proton migration during the complexation reaction results in modifications to the chemical shifts of carbon atoms surrounding reaction sites of the donor and the acceptor. ^{13}C NMR enabled determination of these changes. The [+]NH-linked carbon appeared in the spectrum of the complex at 101.5 ppm and in the spectrum of the free acceptor at 111 ppm. Similarly, the N[-]-linked carbon (C=O) of GLC in the spectrum of the complex appeared at 152.32 ppm, whereas in the spectrum of the free donor it appeared at 151.5 ppm (Figure 8B in the electronic supplementary materials). On the other hand, the change in the ^{13}C NMR chemical shifts for the two aromatic ring carbons of the reagents (much more for the DDQ) confirms the π→π* interaction between the GLC and DDQ.

GLC also reacts with TCNE as a π-acceptor, and the interaction sites are different from those described above (Figure 9A in the electronic supplementary materials). The protons of CO–NH–N and SO$_2$–NH–CO have not undergone any significant changes, confirming that the acceptor-donor interaction was far from these two sites. On the other hand, the protons bound to the carbon atoms located on either side of the nitrogen atom of the azabicyclooctyl ring of GLC appeared with new chemical shifts (Figure 9A in the electronic supplementary materials). In addition, the appearance of a new signal at 4.45 ppm confirms the replacement of one of these hydrogen atoms due to the TCNE missing one of its cyano groups (one of the TCNE C≡N groups was removed by the substituted hydrogen atom, removing HCN, Formula 2, (Figure 2B)). Following the substitution of one of its protons by the CN–C=C–(CN$_2$) motif (Tricyanoethylene), the equivalence of the remaining hydrogen atoms was affected and, consequently, the displacements changed and a new peak appeared, corresponding to the remaining neighboring proton.

The ^{13}C NMR spectrum of the complex [(GLCTCNE)] shows that this interaction has influenced the neighboring carbon interaction sites, i.e. the change in the environment has led to changes in the chemical shifts of all the other signals of the azabicyclo-octyl ring carbons, GLC, and the acceptor (Figure 9B in the electronic supplementary materials).The other carbon signals are consistent with the proposed molecular structures of these complexes.

From the results, mechanisms were proposed for the GLC reactions with DDQ and TCNE, and these are shown in Figure 2.

(A)
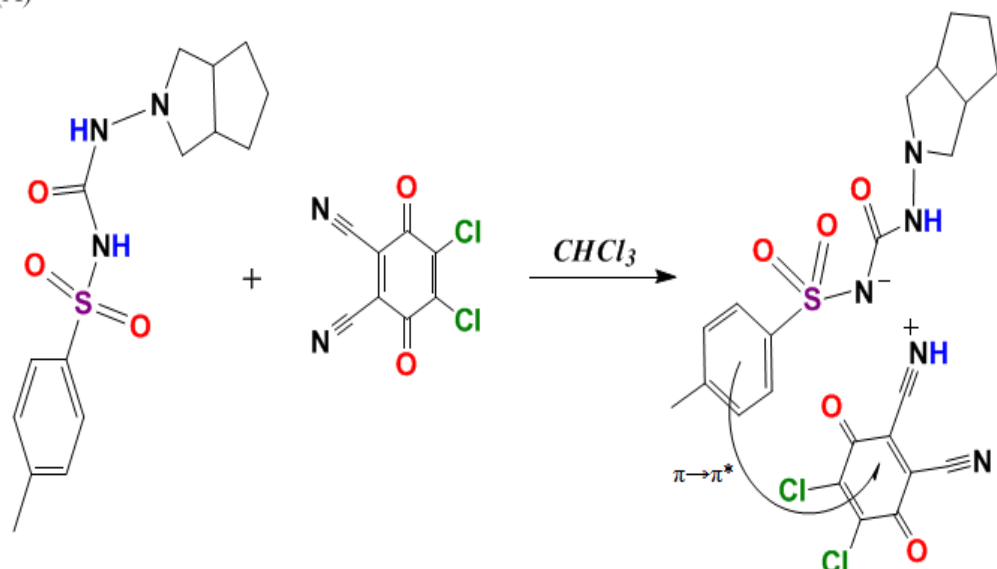
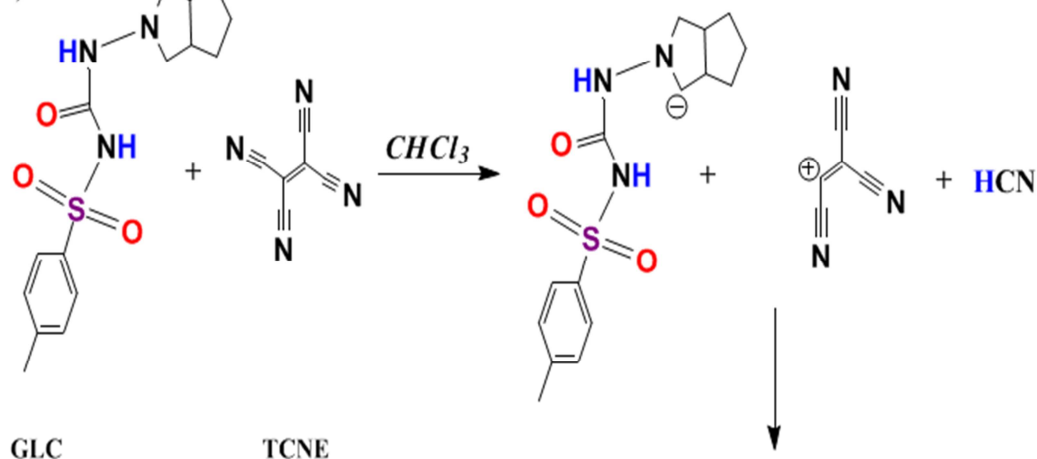GLC   DDQ   Formula (1)
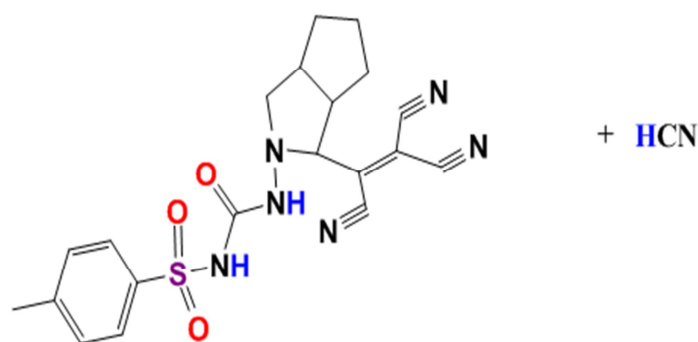   1:1 Charge transfer complex of GLC : DDQ

(B)

GLC   TCNE

Formula (2)   4-methyl-N-(1-(1,2,2-tricyanovinyl)hexahydrocyclopenta[c]pyrrol-2(1H)-
   ylcarbamoyl)benzenesulfonamide

Fig. 2.

3.2.3. DSC measurements

DSC analysis was used to compare the thermal behaviors of the free donor and acceptor with those of their corresponding CT complexes. The DSC thermogram of a molecule has characteristic points depending on temperature. When a donor and an acceptor associate to form a CT complex, a shift, disappearance of characteristic peaks of the free molecules, or appearance of new signals is observed.

Figure 3 shows the thermograms of the donor, acceptors, and their complexes. The endothermic peaks at 170.09°C, 210.58°C, and 197.83°C correspond to the melting points of GLC, DDQ, and TCNE, respectively. It is important to note that the thermal profiles of the complexes are different from those of the free reactants. We observed a change in the characteristic melting points of the complexes (218.87°C for [(GLCTCNE)]) and disappearance of a melting point in region 25–180°C for the complex [(GLC)(DDQ)].This confirms the formation of new interactions between the donor and the acceptors.
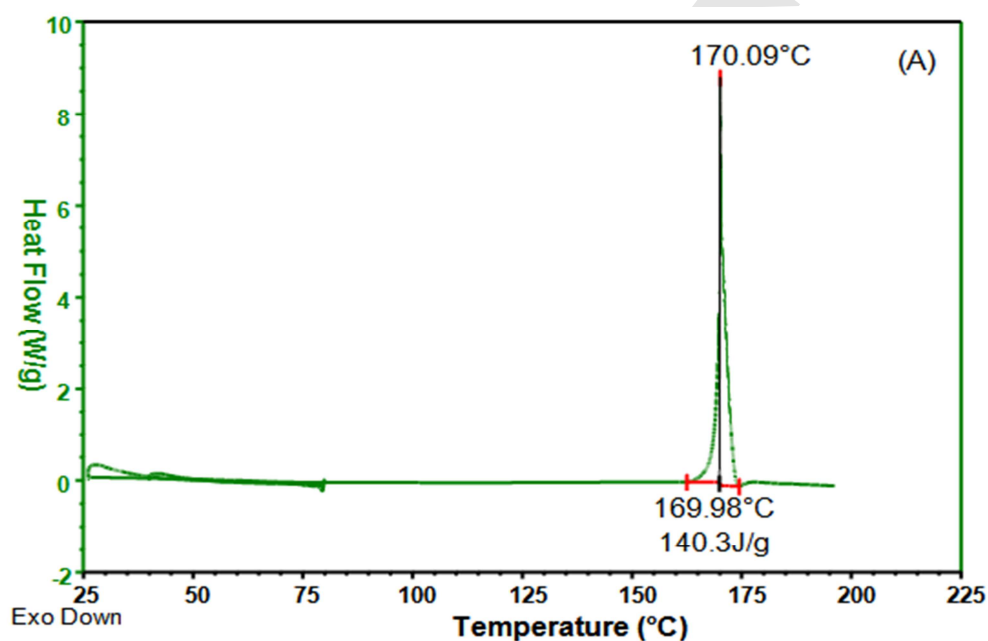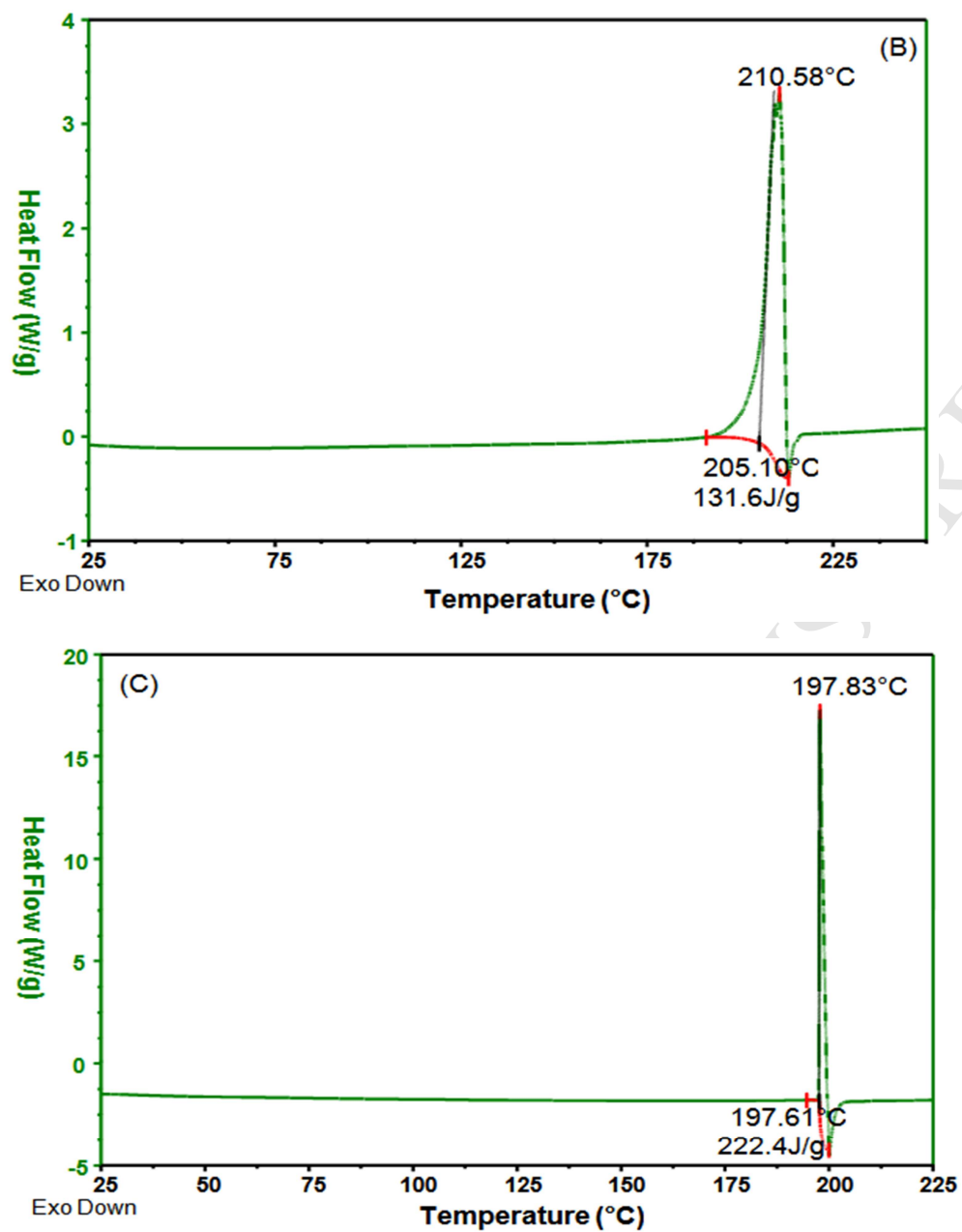
Fig. 3.

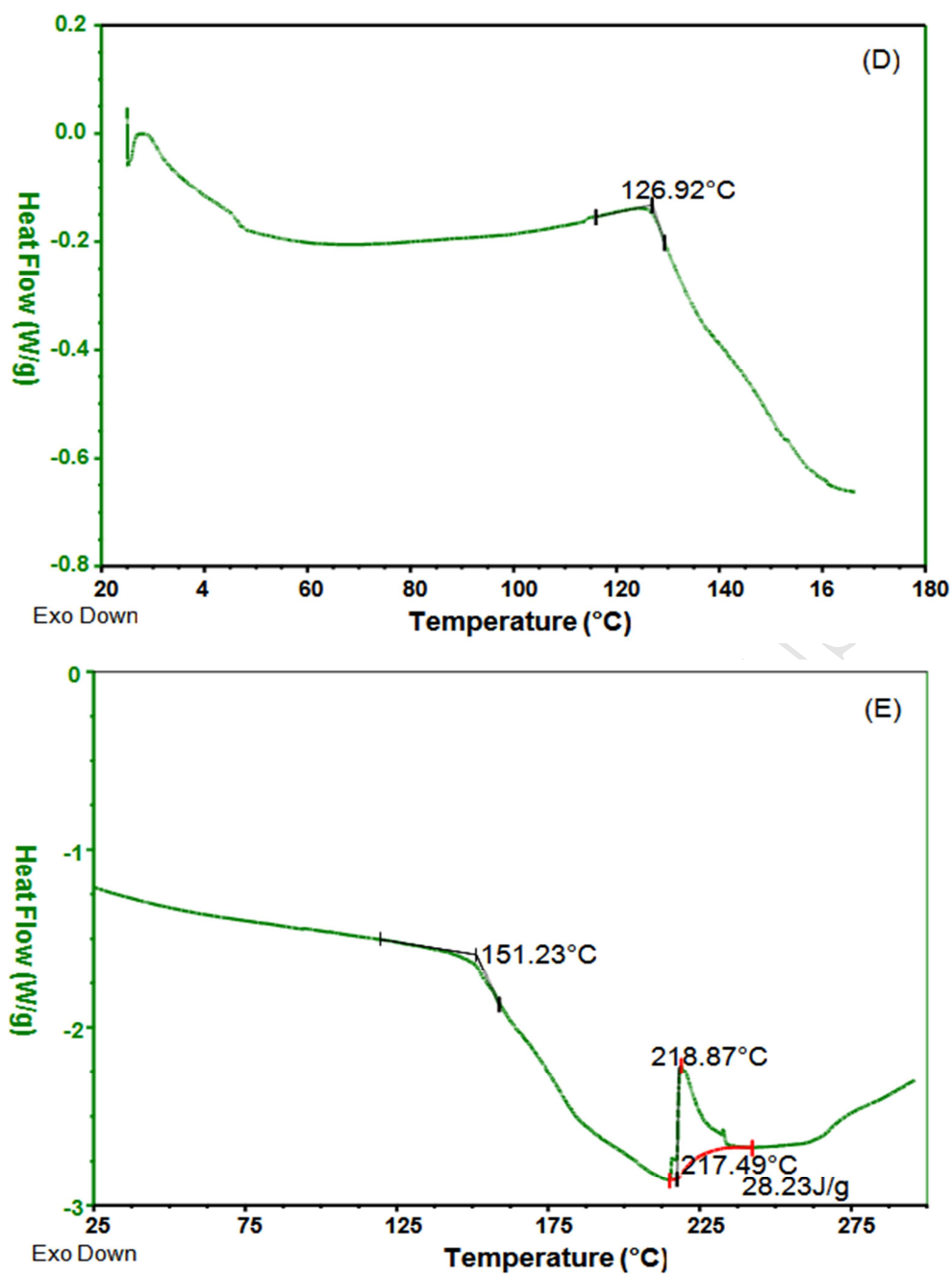### 3.2.4. TGA/DTA measurements

Figure 4 shows the thermogravimetric analysis (TGA/TDA) of the donor, acceptors, and CT complexes performed by increasing the temperature with a heating rate of 10 °C min^{-1} over the temperature range of 25–600 °C. The masses used were 2.80, 4.31, 2.46, 2.66, and 7.69 mg for GLC, DDQ, TCNE, [(GLC)(DDQ)], and [(GLCTCNE)], respectively.

16

Figure 4D shows the decomposition of the complex [(GLC)(DDQ)], which takes place in the following two main steps: the first between 50 and 250°C, which is characterized by endothermic peaks at 119.68°C, 161.82°C, 180.44°C, and 210.16 °C, and the second between 250 and 450°C, which has a peak at 266.19°C. The first step of decomposition is attributed to the degradation of the donor and the evaporation of SO_2, $3NH_3$, CO, CH_4, and $3.5H_2$, with a 29.782% reduction in weight, close to the calculated value of 30.15%. In the second step, DDQ decomposed (observed=18.12 %, calculated=17.26 %) through the elimination of Cl_2 and HCN. The carbon atom residue formed does not undergo decomposition due to the lack of necessary oxygen.

The proposed mechanism for the thermal decomposition of this complex is illustrated as follows:

$$[(GLC)(DDQ)] \xrightarrow{119.68°C,} (GLC) + (DDQ)$$
$$(GLC) \xrightarrow{161.82°C, 180.44°C, 210.16°C} Decomposition$$
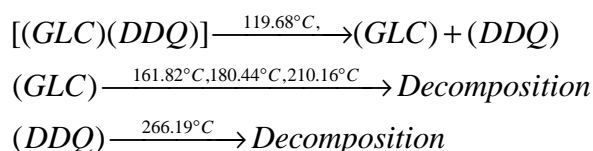$$(DDQ) \xrightarrow{266.19°C} Decomposition$$

Figure 4E shows the TGA/TDA thermogram of the [(GLCTCNE)] complex. Decomposition occurs with a mass loss over five stages between 50 and 150°C, 150 and 220°C, 220 and 290°C, 290 and 390°C, and 390 and 550°C, corresponding to endothermic peaks at 107.43°C, 209.84°C, 275.01°C, 304.9°C, and 440.14 °C, respectively. These are attributed to the loss of the $[C_{20}H_{20}N_6S]$ molecule as $3NH_3$, $3HCN$, SO_2, CO, and $4C_2H_2$. These steps are associated with a total weight loss of 79.24%, which is in agreement with the calculated value (77.26%).
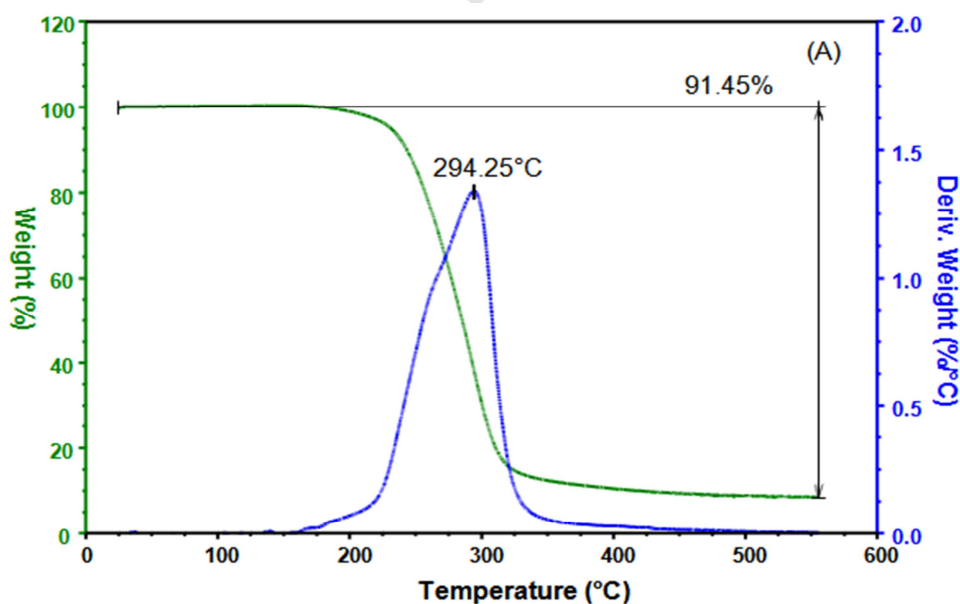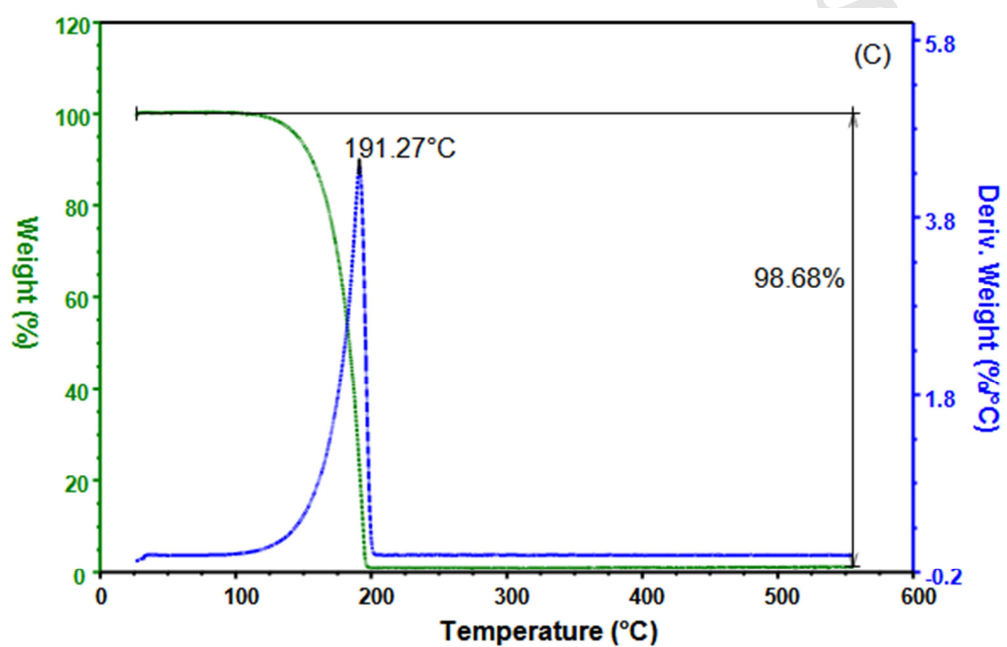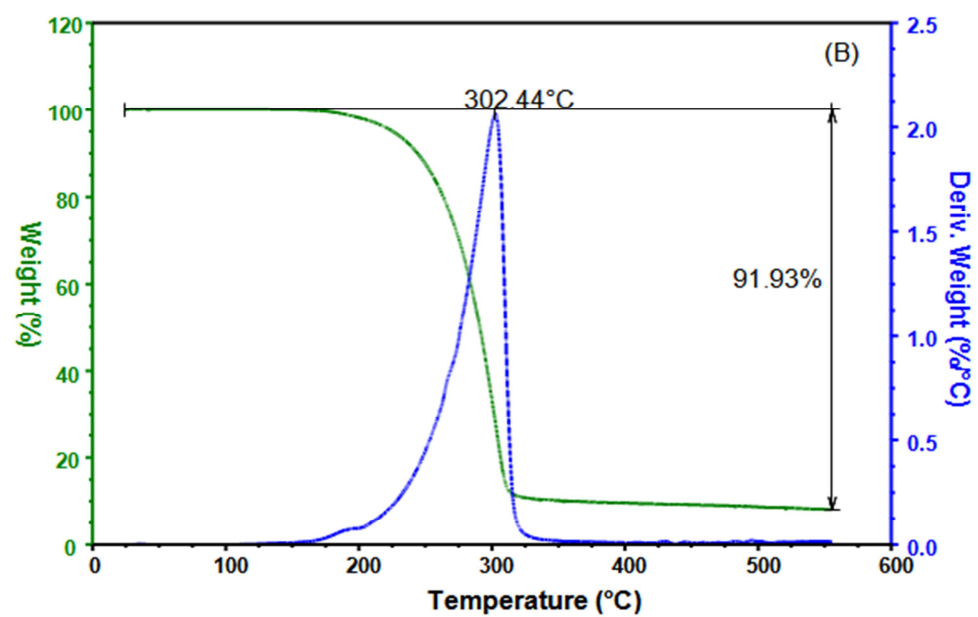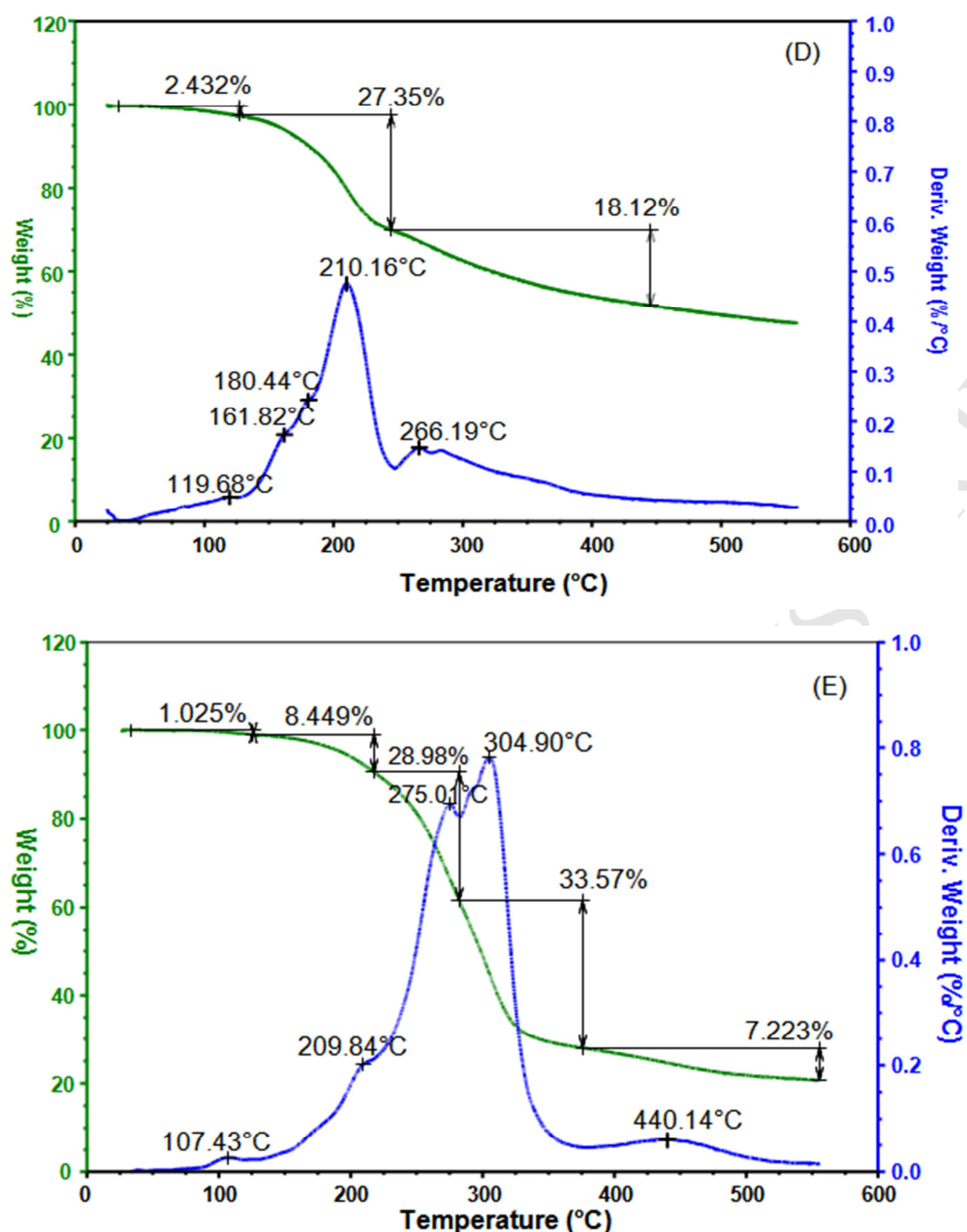
Fig. 4.

3.2.5. Kinetic parameters

In recent years there has been an increased interest in the rate-dependent parameters of solid-state non-isothermal decomposition reactions by analysis of the TGA curves.

These parameters are generally represented by the activation energy (E*), the enthalpy of activation (ΔH*), the entropy of activation (ΔS*), and the free energy of activation (ΔG*), as well as the frequency factor (Z). The parameters were evaluated graphically (Figure 10 in the electronic supplementary materials) using the Coats-Redfern relationship [68]:

$$\ln\left[\frac{-\ln(1-\alpha)}{T^2}\right] = \ln\left(\frac{ZR}{\varphi E}\right) - \frac{E}{RT}$$

(11)

where α is the fraction of the sample decomposed at time t, φ is the linear heating rate, T is the derivative peak temperature, R is the gas constant, and E* is the activation energy. A plot of the left side versus 1/T gives a slope for the evaluation of the activation energy E* in kJ mol⁻¹. The Z (s⁻¹) value was calculated from the intercept (Figure 10 in the electronic supplementary materials).The other kinetic parameters, ΔH*, ΔS* and ΔG* were computed using the following relationships:

$ΔS* = Rln\ (Zh/kT_m)$ (12)

$ΔH* = E - RT_m$ (13)

$ΔG* = ΔH* - T_mΔS*$ (14)

where k is the Boltzmann's constant, h is Planck'sconstant, and T_m is the DTA peak temperature.

The kinetic data obtained from the non-isothermal decomposition of the complexes are given in Table 3. A higher value of activation energy indicates higher thermal stability. The [(GLC)(DDQ)] complex exhibited a higher activation energy value. Therefore, E* for the [(GLCTCNE)] complex is higher compared with the [(GLC)(DDQ)] complex, indicating the higher thermal stability of this complex.

The negative values of ΔS* observed for the two complexes indicate that the reaction rate is slower than normal.

Correlation coefficients from the Arrhenius plots of the thermal decomposition steps were observed to be r~1 for both cases, suggesting a good fit with the linear function and reasonable agreement between the kinetic parameters and the experimental data.

Table 3.

Compounds	E (KJ mol⁻¹)	Z (s⁻¹)	ΔS (J mol⁻¹ K⁻¹)	ΔH (KJ mol⁻¹)	ΔG (KJ mol⁻¹)	R
[(GLC)(DDQ)]	22.11	529.72	-196.68	18.09	113.12	-0.988
[(GLCTCNE)]	40.48	1.49×10^4	-170.43	36.46	98.491	-0.998

3.3. Molecular modeling studies

After conducting the experimental studies that demonstrated the nature of the interaction mechanism between GLC and TCNE, and to prove this interaction, we have conducted DFT and TD-DFT calculations. The calculations were conducted on more simplified structures, where the proton of the proton atoms bound to the carbon atoms located on either side of the nitrogen atom of the azabicyclooctyl ring of GLC was replaced by the pattern C_5N_3 (tricyanoethylene). Two possible conformers for [(GLCTCNE)] are illustrated in (Figure 11 in the electronic supplementary materials). The energies of two [(GLCTCNE)] conformers calculated by the DFT method are -1726.780016 and -1726.671861 Hartrees for S1 and S2, respectively. From this calculation, the conformer S1 (Figure 5) is predicted to be more stable than the other conformer.
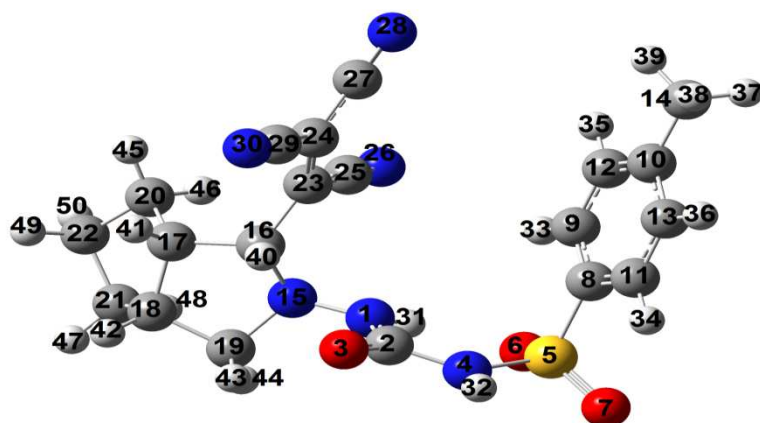
Fig. 5.

3.3.1. UV-Visible

The computation UV-Visible spectrum was studied to obtain the nature of the transitions, electronic excitation energies, and oscillatory strength by using the TD-DFT method. The calculated electronic transitions of high oscillatory strength are given in Table 4, and the simulated spectrum is shown in (Figure 12 in the electronic supplementary materials). The calculated values of λ_{max}= 359.59 nm, f= 0.013, λ_{max}= 271.57 nm, f= 0.0671, λ_{max}= 266.93 nm, and f= 0.0435 are in agreement with the observed electronic transitions at 334 and 259 nm, respectively. The molecular orbital coefficient analyses (Figure 13 in the electronic supplementary materials) confirm that these electronic excitations are n→π* and π→π*.

Table 4.

S. No.	Excitations	E (eV)	(f)	λ_{max} calcd.	λ_{max} obs.	Assignment
1	111 ->112 (H…L)	3.4480	0.0130	359.59	334	n→π*
2	110 ->112 (H-1…L)	4.5654	0.0671	271.57	259	n→π*
3	108 ->112 (H-3…L)	4.6449	0.0435	266.93		π→π*

3.3.2. Vibrational assignments

The vibrational wavenumbers and the appropriate description of each normal mode were obtained using the DFT/B3LYP method employing the basis set 6-311++G (d, p) for the most stable structure, S1, which is summarized in Table 5. The fundamental modes were attributed by comparing the calculated results with the experimental values. The calculated wavenumbers were slightly higher than the values observed for the majority of the normal modes. Two factors may be responsible for the discrepancy between the experimental and calculated spectra of this compound. The first reason is due to the environment and the second reason is due to the fact that the experimental value is ananharmonic wavenumber, while the calculated value is a harmonic wavenumber. Experimental and theoretically predicted FT-IR spectra for S1 are shown in (Figure 14 in the electronic supplementary materials).

Table 5.

Observed wavenumber (cm-1)	B3LYP/6-311++G (d, p) Calculated wavenumber	Assignments
664.35	660.31	νS5 –C8
690.57	686.59	ρCH_2 H46–C28–H45 + H48–C21–H47
705.28	705.28	δCCC C23–C24–C27
751.19	756.29	δNCN N4–C2–N1
811.85	811.20	δCCC C11–C8–C9 + C13–C10–C12
882.00	870.15	ν_sCNC C16–N15–C19
896.81	886.66	ν_s C16–C17–C18
918.07	911.50	ρCH_2 H45–C20–H46; H47–C21–H48 +BC22–H49
949.50	923.49	ν_s C21–C22–C20
995.59	996.19	γCH of benzene ring
1010.90	1011.20	ν_s N1–C2–N4 + ρCH_3
1020.58	1024.45	βCH of azabicyclo-octyl ring
1040.25	1059.37	γCH of azabicyclo-octyl ring
1087.31	1066.88	$\nu s\ SO_2$
1160.96, 1434.64	1188.15, 1330.29	ν C16–N15

1217.03	1217.15	γCH of azabicyclo-octyl ring
1229.79	1230.50	νC10–C14
1290.83	1290.86	τCH$_2$ H45–C20–H46; H47–C21–H48 + γCH C17–H41; C18–H42; C19–H43
1299.91	1305.29	τHCCH H41–C17–C18–H42 + γCH C16–H48; C20–H45; C19–H44
1309.72	1310.85	γCH of azabicyclo-octyl ring +β NH
1345.71	1310.93	ν_{as} SO$_2$
1596.57, 1634.79	1600.44, 1632.41	ν C=C
1708.51	1745.89	νC=O
2300.87	2325.60	ν_s C≡N N26≡C25–C23=C24–C29≡N30
2201.50	2335.48	ν_{as} C≡N N30≡C29 –C24=C27≡N28 + ν C25≡N26
2170.78	2348.27	ν_s C≡N N30≡C29 –C24=C27≡N28 + ν C25≡N26
2837.38	3020.88	ν C16–H40
2867.66	3023.88	ν_s CH$_3$
2948.73	3085.94	ν_{as} CH$_3$
2969.70	3100.43, 3090.15	ν CH of azabicyclo-octyl ring
3110.89	3115.78	ν_{as} CH$_2$ of CH$_3$ H39–C14–H38
3192.02	3178.43, 3174.71	ν CH benzene
3269.66	3541.49, 3517.40	νNH N1–H31, νNH N4–H32

ν- stretching; β- in plane bending; δ- deformation; γ- out of plane bending; ω- wagging; τ- twisting and ρ-rocking

C–H vibrations

The C–H stretching vibrations of azabicyclo-octyl and benzene rings are assigned in the region 3192.02–2969.70 cm^{-1}. The calculated C–H stretches of benzene at 3178.43 and 3174.71 cm^{-1} correspond to the observed wavenumber at 3192.02 cm^{-1} experimentally. These ν C–H vibrations also correspond to the C–H stretching vibrations for aromatic compounds (Ar–ν$_{C–H}$) reported in the literature in the region of 3100–3000 cm^{-1} [69, 70]. The C–H stretches of azabicyclo-octyl was observed experimentally at 2969.70 cm^{-1}. This band was assigned at 3100.43 and 3090.15 cm^{-1} in the theoretical IR spectrum.

In-plane (β) and out-of-plane (γ) C–H bending vibrations are reported in the literature in the region of 1300–1000 and 900–675 cm^{-1}, respectively [71]. The scaled theoretical values of in-plane (β) and out-of-plane (γ) C–H bending vibrations coincide well with that of experimental data, as depicted in Table 5. According to the internal coordinate system recommended by Pulay et al. [72], the calculated band at 1337.91 cm^{-1} is demonstrated by the wagging mode of the CH$_2$ group, and is observed at 1345.71 cm^{-1}, experimentally.

The C–H methyl group stretching vibrations are generally observed in the range 3000–2800 cm^{-1} [73, 74]. The observed CH$_3$ symmetrical ν$_s$ and asymmetrical ν$_{as}$ stretching vibrational bands at 2867.66 and 2948.73 cm^{-1} agree with the calculated wavenumbers at 3028.16 and 3085.94 cm^{-1}. A weak band for CH$_2$ stretching associated with C14 as the methyl carbon atom (ν H39–C14–H38) (Figure 5) was assigned at 3115.78 cm^{-1} in the theoretical IR spectrum, whereas this is very close to the observed experimental wavenumber at 3110.89 cm^{-1}.

N–H vibrations

The N–H stretching vibration appears as a strong band in the region around 3500–3300 cm^{-1} [75, 76]. In this study, the N–H stretching band was observed in the FT-IR spectrum at 3269.66 cm^{-1}. The corresponding theoretical wavenumber for N–H stretching vibrations (ν N1–H31) and (ν N4–H32) (Figure 5) are at 3541.17 cm^{-1} and 3571.40 cm^{-1}, respectively, which shows a positive deviation of ∼ 270 cm^{-1} from the experimental value. This may be due to the presence of inter-hydrogen bonding.

S=O and C=O vibrations

In the experimental FT-IR spectrum, the symmetric and asymmetric stretching vibrations of SO$_2$ observed at 1160.96 and 1345.71 cm^{-1} are in agreement with the calculated wavenumbers of the title molecule at 1310.93 and 1066.96 cm^{-1}. The C=O stretching vibration has a very intense and narrow peak in the range of 1800–1600 cm^{-1} [77, 78]. For the title molecule, the

24

C=O stretching vibration was observed at 1708.51 cm^{-1}. This is in good agreement with the calculated value at 1745.90 cm^{-1} in the theoretical IR spectrum.

C≡N, C–N, and N–N vibrations

The C≡N stretching frequency is localized within the tricyanoethylene group (Figure 5). The characteristic frequency of the C≡N stretching vibration [73, 79, 80] falls in the region of the 2220–2240 cm^{-1} spectral range. For the title compound, the observed bands at 2300.87, 2201.50, and 2170.78 cm^{-1} are due to the C≡N stretching vibration. The corresponding DFT calculations at 2325.60, 2335.48, and 2348.27 cm^{-1}, respectively yields a positive deviation according to the observed results. According to Silverstein et al. [81], the C–N absorption band occurs in the region 1382–1266 cm^{-1}. For the title molecule, the strong C–N stretching modes were observed at 1434.64 and 1160.96 cm^{-1} in the FT-IR spectrum. These bands are in agreement with the calculated bands at 1330.26 and 1188.16 cm^{-1}. The calculated wavenumber at 1199.66 cm^{-1} demonstrates a combination band of the N–N stretching vibration (ν N1–N15) (Figure 5), which is also in agreement with the reported band in the literature at 1107 cm^{-1} [82].

C=C and C–C vibrations

The ring C=C stretching vibrations usually occur in the region 1625–1430 cm^{-1} [83]. In the present study, the C=C stretching vibrations of the aromatic ring and the tricyanoethylene (C23=C24) (Figure 5) were observed at 1634.79 and 1596.57 cm^{-1}, respectively, and are in good agreement with the calculated values at 1632.41 and 1600.58 cm^{-1}. The ring deformation mode generally occurs in the region around 943–923 cm^{-1} [84]. The bands observed at 1028.16 and 811.85 cm^{-1} are assigned to ring torsion modes, and their corresponding calculated values are 995.59 and 811.20 cm^{-1} [85]. The mode that occurred at 1229.79 cm^{-1} in the FT-IR spectrum is assigned to the C–C bending vibration, and the computed value is 1230.50 cm^{-1}.

C–S vibrations

The C–S stretching bands are usually observed in the range 930–670 cm^{-1} [86, 87], with a moderate intensity. For the title compound, the C–S stretching mode observed at 664.35 cm^{-1} agrees well with the computed at 660.31 cm^{-1}. The C–S in-plane and out-of-plane bending vibration bands are expected in the regions 550–420 cm^{-1} and 420–320 cm^{-1}, respectively [86]. In the present investigation, the C–S in-and out-of-plane bending vibrations are assigned

25

to 424.52 and 327.42 cm^{-1}, respectively. All the C–S vibrational bands of S1 are in line with the characteristic regions and are in agreement with the computed values.

3.3.3. ^{1}H and ^{13}C NMR

The theoretical ^{1}H and ^{13}C NMR chemical shifts of S1 have been compared with the experimental spectra, as shown in Table 6. Chemical shifts are reported in ppm relative to TMS for ^{1}H and ^{13}C NMR spectra. The atom statues were numbered according to Figure 5. The calculated chemical shift values of 7.70, 7.92, and 2.38 ppm for the aromatic and methyl hydrogen atoms (H35,36, H33,34, H37,38, and 39) are in good agreement with the measured values (7.40, 7.72, and 2.39 ppm). The protons of the azabicyclooctyl ring are observed in the range of 1.12–4.45 ppm, while these peaks are calculated in the range of 1.43–5.29. The signals due to the hydrogen atoms H31and H32, which bind to the nitrogen atoms, are observed at 8.10 and 6.10 ppm, whereas these are calculated at 7.96 and 5.89 ppm in the theoretical ^{1}H NMR spectrum. Aromatic carbon signals are between 100 and 150 ppm in organic molecules [88, 89]. The signals due to aromatic carbons C8, C9, C11, C12, C13, and C10 are observed at 144.20, 129.59, 127.40, and 136.29 ppm, respectively, in DFT calculations. These signals are predicted at 145.76, 131.43, 135.08, and 155.05 ppm. The signal due to the carbon which binds to oxygen is observed at 151.90 ppm, while it is calculated at 156.04 ppm in the theoretical ^{13}C NMR spectrum. The signals at 169.80, 112.03, 125.58, and 121.14 ppm due to carbons C23, C24, C25, C27, and C29 are in agreement with the calculated values at 166.81, 103.39, 120.85, 116.49, and 115.41 ppm respectively. The other carbon atoms of the azabicyclooctyl ring are observed in the range of 30.57–72.11 ppm, which is consistent with the predicted ^{13}C NMR spectrum. The relation between the experimental ^{1}H and ^{13}C NMR (δ_{exp}) and calculated (δ_{calc}) chemical shifts is generally linear and described by the following equation [90]:

$$\delta_{exp} = a + b\, \delta_{calc} \tag{15}$$

The slope and intercept at the origin of the least squares correlation were used to predict chemical shifts, and the linear correlation coefficient (R) was used to verify the accuracy and agreement between experimental and theoretical data. In this study, the correlation coefficients for the chemical shifts of the proton and carbon were 0.979 and 0.983, respectively. This proves an agreement between the experimental data and their calculated data (Figure 6).

Table 6.

| Atom	Experimental	B3LYP/6311++G (d, p)
¹H NMR		
H33, H34	7.74	8.03, 7.92
H31	8.10	7.96
H35, H36	7.40	7.62, 7.70
H32	6.10	5.89
H40	4.45	5.29
H43	3.56	3.89
H41	2.94	3.03
H44	3.43	2.91
H42	2.67	2.71
H37, 38, 39	2.39	2.57, 2.38, 2.34
H50	1.51	1.56
H45, 47	3.15	1.65, 2.12
H46, 48	1.12	1.61, 1.44
H49	1.40	1.43
¹³C NMR		
C23	169.80	166.81
C2	151.90	156.04
C10	136.29	155.05
C8	144.20	145.76
C12, C13	127.40	135.08, 136.23
C9, C11	129.25	131.43, 131.11
C25	125.58	120.85
C27, 29	121.14	116.49, 115.41
C24	112.03	103.39
C16	72.11	73.05
C19	61.84	58.81
C17	52.80	55.37
C18	49.17	46.66
C22	23.99	32.16
C20, C21	30.57	31.35, 38.84
C14	21.02	21.58
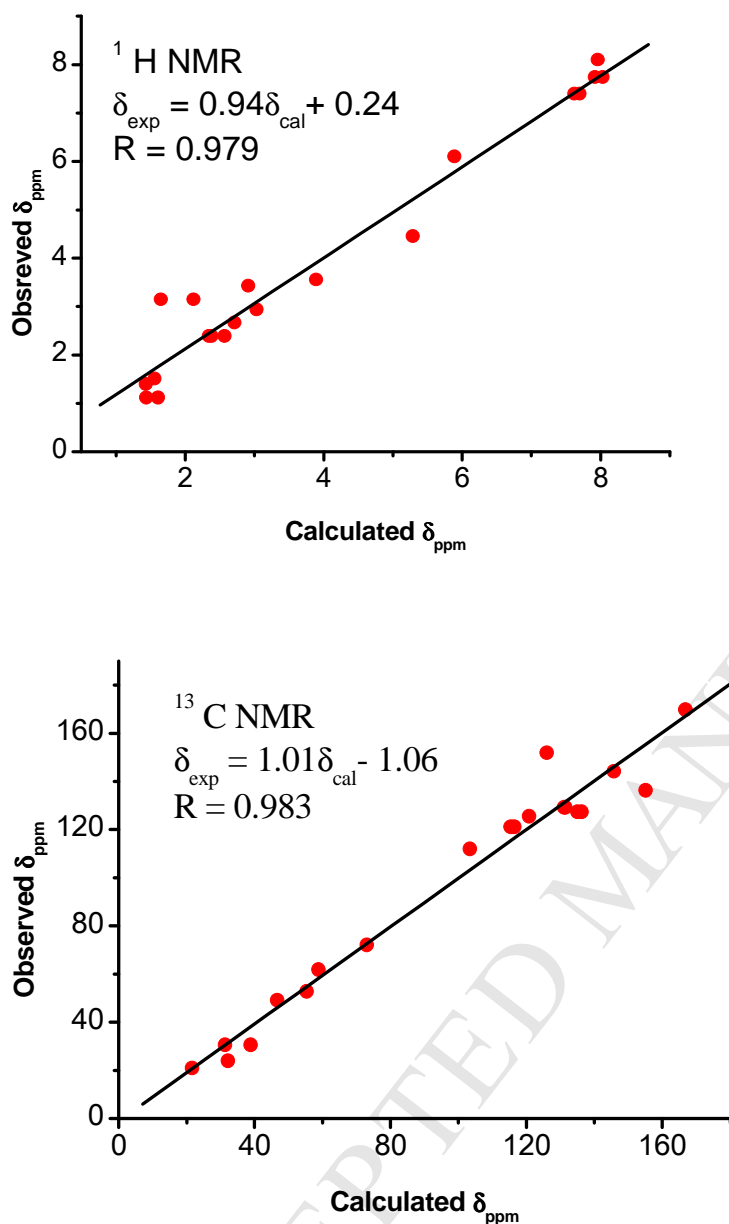
Fig. 6.

4. Conclusion

The formation of GLC charge-transfer complexes with both acceptors DDQ, and TCNE was confirmed in solution and in the solid state. In solution, the formation of CT complexes was visualized by UV-vis spectroscopy. The appearance of absorbing bands at 266 nm for (GLC-DDQ) and 259 nm for (GLC-TCNE) confirms the formation of new species. The stoichiometry of the formed complexes determined by photometric titration was 1:1. The calculated stability constants of the two complexes at different temperatures were used to

determine the thermodynamic parameters, based on whether the reactions were exothermic ($\Delta H° < 0$) and spontaneous ($\Delta G° < 0$).

The UV-vis spectra were used to determine the oscillator strength (*f*), transition dipole moment (μ_{EN}), and ionization potential (I_P).

The LOD and LOQ values indicated that the proposed methods can be used to successfully determine GLC in pharmaceutical formulations.

Characterization of the solid-state complexes by FT-IR, ^{1}H NMR, and ^{13}C NMR confirms the existence of a $\pi \rightarrow \pi^*$ interaction associated with the migration of the GLC proton to the DDQ acceptor for the complex [(GLC)(DDQ)], and a covalent interaction between GLC and TCNE. Changes in the thermal profiles and melting points on the DSC thermograms of the complexes versus the free reagents indicated the formation of new interactions between the donor and the acceptors.

The thermogravimetric analysis (TGA/DTA) showed the degradation steps of the free reagents and the complexes. The decomposition data allowed us to calculate the kinetic parameters (ΔG^*, ΔH^*, and ΔS^*) using the Coats-Redfern method.

Density functional theory (DFT) studies confirmed the mode of interaction between the GLC and the TCNE by comparing the theoretical results obtained with the experimental data. Harmonic vibration frequencies, and ^{1}H NMR and ^{13}CNMR chemical shifts were obtained by the DFT/B3LYP methods using a 6-311++G (d, p) basis set, in accordance with the experimental results. The theoretical UV-visible spectrum of the compound and the electronic properties, such as the HOMO and LUMO energies, were realized using the TD-DFT approach with CAM-B3LYP and a 6-311++G (d, p) basis set, and were in good agreement with the theoretical and experimental UV-visible data found.

References

[1] A. M. A. Adam, M. S. Refat, J. Mol. Liq. 209 (2015) 33–41.

[2] A. Amer, M. Abounassif, H. AlRabiah, G. Abdel-Haiz Mostafa, Trop J Pharm Res 15 (2016) 995–1001.

[3] A. Al-Badr, G. A.-H Mostafa, Trop J Pharm Res 12 (2013) 1057–1063.

[4] T. S. Belal, D. S. El-Kafrawy, M. S. Mahrous, M. M. Abdel-Khalek, A. H. Abo-Gharam, Spectrochim. Acta Part A 115 (2016) 47–53.

[5] A. Dozal, H. Keyzer, H.K. Kim, W.W. Wang, Int. J. Antimicrob. Agents 14 (2000) 261–265.

[6] M. Pandeeswaran, E.H. El-Mossalamy, E.H. Elango, Int. J. Chem. Kinet 41 (2009) 787–799.

[7] A. Korolkovas. Essentials of Medical Chemistry. 2nd Eds. Wiley, New York, 1998.

[8] M. Pandeeswaran, K.P. Elango, Spectrochim. Acta Part A 75 (2010) 1462–1469.

[9] S. Tunç, O. Duman, B. K. Bozoğlan, J. Lumin. 140 (2013) 87–94.

[10] M. Saravanabhavan, K. Sathya, V.G. Puranik, M. Sekar, Spectrochim. Acta Part A 118 (2014) 399–406.

[11] S. Tunç, A. Çetinkaya, O. Duman, J. Photochem. Photobiol. B 120 (2013) 59–65.

[12] O. Duman, S. Tunç, B. Kanci Bozoğlan, J Fluoresc 23 (2013) 659–669.

[13] B. Kanci Bozoğlan, S. Tunç, O. Duman, J. Lumin. 155 (2014) 198–204.

[14] British Pharmacopoeia, Monograph: Medicinal and Pharmaceutical Substances. Medicines & Health Products Regulatory Agency, UK, 2013, pp. 1022-1023.

[15] S. Baba, S. Nakagawa, K. Takebe, Y. Goto, H. Maezawa , R. Takeda, Clin Eva. 11 (1983) 51–94.

[16] D.B. Campbell, P.I. Adriaenssens, Y.W. Hopkins, B. Gordon, J.R.B. Williams, A review. Royal Soc Med Int Congr Symp 20 (1980) 71–82.

[17] L.L. Chen, F. Yu, T.S. Zeng, Y.F. Liao, Y.M. Li, H.C. Ding, Eur. J. Pharmacol. 659 (2011) 296–301.

[18] A.D. B. Harrower, Diabetes Res Clin Pract 14 (1991) 65–67.

[19] F.A.M. Al-Omary, Gliclazide, Profiles of Drug Substances, Excipients, and Related Methodology. Elsevier Inc, 2017, pp.126-184.

[20] C.S. Winters, P. York, P. Timmins, Eur J Pharm Sci 5 (1997) 209–214.

[21] J.R. Moyano, M.J. Arias-Blanco, J.M. Ginés, F. Giordano, Int. J. Pharm. 148 (1997) 211–217.

[22] J.R. Moyano, M.J. Arias-Blanco, J.M. Ginés, F. Giordano, Int. J. Pharm. 157 (1997) 239–243.

[23] M.J.A Arias-Blanco, J.R. Moyano, J.I.P Martinez, J.M. Gines, J Pharm Biomed Anal 18 (1998) 275–279.

[24] Y. Ozkan, T. Atay, N. Dikmen, A. Isimer, H.Y. Aboul-Enein, Pharm Acta Helv 74 (2000) 365–370.

[25] M. Barzegar-Jalali, H. Valizadeh, M.R. Siahi Shadbad, K. Adibkia, G. Mohammadi, A. Farahani, Z. Arash, A. Nokhodchi, Powder Technol 197 (2010) 150–158.

[26] S.B.G. Basiaga, D.S. Hage, J. Chromatogr.B 878 (2010) 3193– 3197.

[27] R. Matsuda, J. Anguizola, K.S. Joseph, D.S. Hage, Anal Bioanal Chem 401 (2011) 2811–2819.

[28] Y. Yao, W.W. Han, Y. Zhou, Z.S Li, Q. Li, X.Y. Chen, D.F Zhong, Eur. J. Med. Chem. 44 (2009) 854–861.

[29] S.K. Mastan, K.E. Kumar, Int J Diabetes Mellit 2 (2010) 56–60.

[30] H. Banu, N. Renuka, G. Vasanthakumar, Biochimie 93 (2011) 1028–1036.

[31] C.M Sultanpur, S. Satyanarayana, N.S Reddy, K.E Kumar, S. Kumar, J Young Pharm 2 (2010) 152–155.

[32] H. Yao, J. Feng, Q. Zheng, Y. Wei, S. Wang, W. Feng, Life Sci. 161 (2016) 60–68.

[33] G.G. Mohamed, S.M. Abdallah, M.M.I. Nassar, M.A. Zayed, Arab. J. Chem. 2 (2009) 109–117.

[34] B.K. Sharma, S.A. Iqbal, O. Prakash, Chem Materials Res. 3 (2013) 18–27.

[35] M. G. Abd El-Wahed, S. M. El-Megharbel, M. Y. El-Sayed, Y. M. Zahran, M. S. Refat, M.A. Al-Omar, A.M, Naglah, Russian J. Gen. Chem. 86 (2016) 391–399.

[36] M. Shukla, N. Srivastava, S. Saha, J. Mol. Struct. 2012, 1021, 153 M. Shukla, N. Srivastava, S. Saha, J. Mol. Struct. 1021 (2012) 153–157.

[37] M. Ting, N.J.S. Peters, J. Phys. Chem. A. 113 (2009) 11316–11317.

[38] M.S. Refat, H.A. Saad, A.M.A. Adam, J. Mol. Struct. 995 (2011) 116–124

[39] E.M. Nour, S.Y. Alqaradawi, A. Mostafa, E. Shams, H.S. Bazzi, J. Mol. Struct. 980 (2010) 218–224.

[40] L. Brault, E. Migianu, A. Néguesque, E. Battaglia, D. Bagrel, G. Kirsch, J. Med. Chem. 40 (2005) 757–763.

[41] E.M. Nour, M.S. Refat, J. Mol. Struct. 994 (2011) 289–294.

[42] M.S. Refat, A. Elfalaky, E. Elesh, J. Mol. Struct. 990 (2011) 217–226.

[43] D.A. Jose, A.D. Shukla, G. Ramakrishna, D.K. Palit, H.N. Ghosh, A. Das, J. Phys. Chem. B. 111 (2007) 9078–9087.

[44] A.S. AL-Attas, M.M. Habeeb, D.S. AL-Raimi, J. Mol. Struct. 928 (2009) 158–170.

[45] A.A. Fakhro, H.S. Bazzi, A. Mostafa, L. Shahada. Synthesis, spectroscopic and thermal structural investigations of the charge–transfer complexes formed in the reaction of 2-methylpiperidine with σ - and π -acceptors. Spectrochimica Acta Part A 75 (2010) 134–141.

[46] S. Sadeghi, E. Karimi, Chem. Pharm. Bull. 54 (2006) 1107–1112

[47] F.L. Zhao, B.Z. Xu, Z.Q. Zhang, S.Y. Tong, J. Pharm. Biomed. Anal. 21 (1999) 355–360.

[48] A.S. Amin, A.M. El-Beshbeshy, Microchim. Acta 137 (2001) 63–69.

[49] International Conference on Harmonization of Technical Requirements for Registration of Pharmaceuticals for Human Use, ICH Harmonisation Tripartite Guideline, Validation of Analytical Procedures: Text and Methodology: Q2 (R1), Complementary Guideline on Methodology dated 06 November 1996, London, incorporated in November 2005.

[50] D.A. Skoog. Principle of Instrumental Analysis. fifth ed., Saunders College Publishing, New York, 1992.

[51] A. Mostafa, H.S. Bazzi, Spectrochim. Acta Part A 79 (2011) 1613–1620.

[52] M.J. Frisch, G.W. Trucks, H.B. Schlegel, G.E. Scuseria, M.A. Robb, J.R. Cheeseman, G. Scalmani, V. Barone, B. Mennucci, G.A. Petersson, H. Nakatsuji, M. Caricato, X. Li, H.P. Hratchian, A.F. Izmaylov, J. Bloino, G. Zheng, J.L. Sonnenberg, M. Hada, M. Ehara, K. Toyota, R. Fukuda, J. Hasegawa, M. Ishida, T. Nakajima, Y. Honda, O. Kitao, H. Nakai, T. Vreven, J.A. Montgomery Jr., J.E. Peralta, F. Ogliaro, M. Bearpark, J.J. Heyd, E. Brothers, K.N. Kudin, V.N. Staroverov, R.Kobayashi, J. Normand, K. Raghavachari, A. Rendell, J.C. Burant, S.S. Iyengar, J. Tomasi, M. Cossi, N. Rega, J.M. Millam, M. Klene, J.E. Knox, J.B. Cross, V. Bakken, C. Adamo, J. Jaramillo, R. Gomperts, R.E. Stratmann, O. Yazyev, A.J. Austin, R. Cammi, C. Pomelli, J.W. Ochterski, R.L. Martin, K. Morokuma, VG Zakrzewski, G.A. Voth, P. Salvador, J.J. Dannenberg, S. Dapprich, A.D. Daniels, O. Farkas, J.B. Foresman, J.V. Ortiz, J. Cioslowski, D.J. Fox, Gaussian 09, Revision A.1, Gaussian Inc., Wallingford CT, 2009.

[53] R. Dennington, T. Keith and J. Millam Semichem Inc., Shawnee Mission KS, GaussView, Version 5, 2009.

[54] R. Ditchfield, J. Chem. Phys. 56 (1972) 5688– 5691.

[55] M. Belfaragui, A. Seridi, J.Y. Winum, M. Abdaoui, M. Kadri, Spectrochim. Acta Part A 108 (2013) 55–61.

[56] H.A. Benesi, J.H. Hildebrand, J. Am. Chem. Soc. 71 (1949) 2703–2707.

[57] M. V. Rekharsky, Y. Inoue, Chem. Rev. 98 (1998) 1875– 1917.

[58] Y. Inoue, T. Hakushi, Y. Liu, L. H. Tong, B. J. Shen, D.S. Jin, J. Am. Chem. Soc. 115 (1993) 475–481.

[59] H. Tsubomura, R.P. Lang, J. Amer. Chem. Soc. 83 (1961) 2085– 2092.

[60] R. Rathone, S.V. Lindeman, J.K. Kochi, J. Am. Chem. Soc. 119 (1997) 9393–9404.

[61] G. Aloisi, S. Pignataro, J. Chem. Soc. Faraday Trans. 69 (1973) 534–539.

[62] M.H. Irving, T.S. Freiser, West, IUPAC. Compendium of Analytical Nomenclature Definitive Rules. Pergamum Press, Oxford, 1981.

[63] M.S. Refat, J. Mol. Struct. 985 (2011) 380–390.

[64] G.G. Mohamed, S.M. Khalil, M.A. Zayed, M. Abd El-Hamid El-Shall, J. Pharm. Biomed. Anal. 28 (2002) 1127–1133.

[65] A.S. Amin, M.E. Moustafa, Y.M. Issa, Microchem. J. 50 (1994) 6–13.

[66] I. Natori, S. Natori, H. Sekikawa, K. Ogino, J. Polym. Sci. Pol. Chem. 48 (2009) 342–350.

[67] http://www.nmrdb.org/new_predictor/index.shtml?v=v2.17.5

[68] A.W. Coats, J.P. Redfern, Nature 201 (1964) 68–69.

[69] R.M. Silverstein, F.X. Webster. Spectrometric identification of organic compounds. sixth ed., Jon Wiley Sons Inc, New York, 1963, pp. 72-108.

[70] J.B. Lambert, H.F. Shurvell, Lawrence Verbit, R.G. Cooker, G.H. Stout. Organic Structural analysis. 2009, pp. 235

[71] R.M. Silverstein, F.X. Webster. Spectrometric Identification of Organic Compounds. sixth ed., Jon Wiley Sons Inc., New York, 1963, pp. 215–274.

[72] . Pulay, G. Fogarasi, F. Pang, J.E. Boggs, J. Am. Chem. Soc. 101 (1979) 2550–2560.

[73] F.R. Dollish, W.G. Fateley, F.F. Bentely. Characteristic Raman Frequencies on Organic Compounds. John Wiley, New York, 1997.

[74] R.M. Silverstein, G. Clayton Bassler, T.C. Morril. Spectrometric Identification of Organic Compounds. John Wiley, New York, 1991.

[75] M.T. Güllüoğlu, Y. Erdoğdu, Ş. Yurdakul, J. Mol. Struct. 834 (2007) 540– 547.

[76] Y. Erdoğdu, M.T. Güllüoğlu, Ş. Yurdakul, J. Mol. Struct. 889 (2008) 361–370.

[77] G. Varsanyi. Vibrational Spectra of Benzene Derivatives. Academic Press, New York, 1969.

[78] G. Socrates. Infrared and Raman Characteristic Group Wave Numbers – Tables and Charts. Third ed., John Wiley and sons, New York, 2001.

[79] D.L. Vein, N.B. Colthup, W.G. Fateley, J.G. Grasselli. The Handbook of Infrared and Raman Characteristic Frequencies of Organic Molecules. Academic Press Inc, San Diego, CA, 1991.

[80] L.J. Bellamy. The Infrared Spectra of Complex Molecules. Wiley, New York, 1975.

[81] M. Rogojerova, G. Keresztury, B. Jordanova, Spectrochim. Acta Part A 61 (2005) 1661–1670.

[82] R.M. Silverstein, F.X. Webster. Spectrometric identification of organic compounds. sixth ed., Jon Wiley Sons Inc, New York, 1963, pp. 72-108.

[83] A. Teimouri, A.N. Chermahini, K. Taban, H.A. Dabbagh, Spectrochim. Acta Part A 72 (2009) 369–377.

[84] B. Karthikeyan, Spectrochim. Acta Part A 64 (2006) 1083–1087.

[85] C. Sridevi, G. Velraj, J. Mol. Struct. 1019 (2012) 50–60.

[86] G. Socrates. Infrared and Raman characteristic Group Frequencies-Tables and Charts, third ed., Wiley, Chichester, 2001.

[87] N.B. Colthup, L.H. Daly, S.E. Wiberly, Introduction to Infrared and Raman Spectroscopy, third ed., Academic Press, Boston, MA, 1990.

[88] K. Pihlaja, E. Kleinpeter. Carbon-13 Chemical Shifts in Structural and Stereochemical Analysis, VCH Publishers, Deerfield Beach, 1994.

[89] H.O. Kalinowski, S. Berger, S. Braun. Carbon-13 NMR spectroscopy, John Wiley & Sons, Chichester, 1988.

[90] P. Barczynski, A. Komasa, M. Ratajczak-Sitarz, A. Katrusiak, J. Koput, Z. Dega-Szafran, M. Szafra, J. Mol. Struct. 984 (2010) 359–370.

Table 1. Thermodynamic parameters of CT complexes of GLC at 25°C

Table 2. Spectrophotometric data of the GLC CT complexes

Table 3. Kinetic parameters of [(GLC)(DDQ)] and [(GLCTCNE)] CTcomplexes

Table 4. Experimental and calculated electronic excitations of S1: E/eV, oscillatory strength (*f*), (λ_{max} /nm) at TD-DFT/CAM-B3LYP/6-311G ++ (d, p) level

Table 5. Experimental and calculated vibrational frequencies (cm^{-1}) of the title compound

Table 6. Experimental and calculated ^{1}H and ^{13}C NMR chemical shifts (with respect to TMS, all values in ppm) of title compound

Fig. 1. Absorption spectra of GLC (10^{-4} M) in chloroform with various concentrations of (A) DDQ; and (B) TCNE.

Fig. 2. Proposed mechanisms for the reaction of GLC with DDQ and TCNE.

Fig. 3. DSC thermograms of (A) GLC, (B) DDQ, (C) TCNE, (D) [(GLC)(DDQ)], and (E) [(GLCTCNE)].

Fig. 4. Thermograms (TGA/TDA) of (A) GLC, (B) DDQ, (C) TCNE, (D) [(GLC)(DDQ)]; and (E) [(GLCTCNE)].

Fig. 5. B3LYP optimized ground state geometric structure of S1.

Fig. 6. Correlation graphic of calculated and experimental ^{1}H and ^{13}C NMR of the title compound.

Highlights

- Two CT-complexes of donor GLC with the acceptors DDQ, and TCNE are obtained.
- The CT-complexes are characterized through UV-vis, FTIR, ^{1}H, and ^{13}C NMR, and thermal analysis.
- The thermodynamic, kinetic, spectroscopic parameters, LOD and LOQ are calculated.
- DFT and TD-DFT calculations on the GLC-TCNE complex were carried
- UV-vis, FT-IR and NMR spectral analyzes were observed and compared with the calculated results.